Available online at www.sciencedirect.com

jmr&t Journal of Materials Research and Technology

journal homepage: www.elsevier.com/locate/jmrt

Experimental analysis and optimization of abrasive waterjet deep hole drilling process parameters for SS AISI 316L

Bharani Chandar J [a], *N. Lenin* [a,***], *Siva Kumar* [a], *Naveen Kumar Gupta* [b], *Alagar Karthick* [c,h,*], *Rathina Suriyan* [a], *Hitesh Panchal* [d], *Abhinav Kumar* [e], *Anand Patel* [f], *Kishor Kumar Sadasivuni* [g,**]

[a] *Department of Mechanical Engineering, Vel Tech Rangarajan Dr. Sagunthala R&D Institute of Science and, Technology, Tamil Nadu, 600062, India*

[b] *Department of Mechanical Engineering, GLA University, Mathura, India*

[c] *Renewable Energy Lab, Department of Electrical and Electronics Engineering, KPR Institute of Engineering, and Technology, Coimbatore, Tamilnadu, 641407, India*

[d] *Mechanical Engineering Department, Government Engineering College Patan, Gujarat, India*

[e] *Department of Nuclear and Renewable Energy, Ural Federal University Named After the First President of Russia, Boris Yeltsin, 19 Mira Street, Ekaterinburg, 620002, Russia*

[f] *Mechanical Engineering Department, LDRP Institute of Engineering and Technology, Gujarat, India*

[g] *Centre for Advanced Materials, Qatar University, Qatar & Department of Mechanical and Industrial Engineering, PO Box 2713, Doha, Qatar*

[h] *Departamento de Quimica Organica, Universidad de Cordoba, Cordoba, Spain*

ARTICLE INFO

Article history:
Received 27 May 2023
Accepted 6 September 2023
Available online 13 September 2023

Keywords:
Deep hole drilling
Abrasive waterjet
Material removal rate
Roundness
Optimization

ABSTRACT

Recent breakthroughs in component downsizing and miniaturization emphasise the requirement for deep-hole drilling with an increased aspect ratio, especially in the automobile sector for fuel injectors and the medical sector for manufacturing bone screws or surgical equipment. In this research, deep hole drilling on stainless steel AISI 316L has been conducted using an Abrasive Waterjet Machine (AWJM), and the influence of drilling variables on the material removal rate, roundness deviation of drilled holes have been evaluated to assess the machining and hole characteristics. In addition, machining parameters' statistical relevance has been investigated using a multi-parametric analysis of variance. Quadratic mathematical models for material removal rate and roundness deviation have been established by correlating drilling parameters. The Grey Wolf Optimization (GWO) algorithm has been applied in this research to identify the optimal combination of deep hole drilling parameters for maximizing material removal rate and minimizing the roundness deviation. The results have been compared with Derivative-free optimization, Whale optimization, and Harmony search

* Corresponding author. Renewable Energy Lab, Department of Electrical and Electronics Engineering, KPR Institute of Engineering, and Technology, Coimbatore, Tamilnadu, 641407, India.
** Corresponding author.
*** Corresponding author.
E-mail addresses: j.bharanichandar@veltech.edu.in (B. Chandar J), n.lenin@gmail.com (N. Lenin), Naveen.kumar@gla.ac.in (N.K. Gupta), karthick.power@gmail.com (A. Karthick), drabhinav@ieee.org (A. Kumar), anand.patel@hcl.com (A. Patel), kishorkumars@qu.edu.qa (K.K. Sadasivuni).
https://doi.org/10.1016/j.jmrt.2023.09.045

algorithms. The comparison revealed that the GWO algorithm performed better than other algorithms. In addition, a validation test has been carried out to confirm the accuracy of the results produced by the GWO. The images obtained from the scanning electron microscope showed that the surfaces of the deep holes are smooth. Additionally, the ploughing action was shown to be the principal mechanism responsible for removing the material.

1. Introduction

Abrasive Waterjet Machining works by directing high-pressure water from a pump into an orifice in the cutting head, where it is accelerated into a high-velocity jet. When water flows through a mixing chamber, it creates a vacuum that pulls abrasive particles into a focusing tube, which combines to form an abrasive waterjet mixture [1]. The material removal mechanism from the target material in AWJM by an erosion process. Material erosion occurs in two different methods such as cutting and deformation [2]. The erosion mechanism varies according to the workpiece material and its properties. For ductile material, material removal occurs by plastic deformation, whereas crack propagation and chipping are applied for brittle materials [3,4]. AWJM offers numerous benefits as compared to other modern manufacturing methods, such as the ability to machine hard-to-cut materials such as Inconel, monal, titanium, and steel, with the capacity to generate contour profiles in workpiece thicknesses ranging from 100 mm to 120 mm for steel and aluminium respectively. Any 2-D profile can be cut with excellent precision. Heat is absent due to no physical contact between the tool and the workpiece material [5]. By recycling and reusing the abrasives, AWJM becomes the most cost-effective, efficient, and ecologically responsive [6].

Veerappan et al. [7] examined the effectiveness of nickel-based superalloys using abrasive waterjet machining. Cutting parameters like Waterjet Pressure (WP), Abrasive Mass Flow Rate (AFR), Stand-off Distance (SoD), and Traverse Speed (TS) were utilized as process variables to study surface integrity and rate of material removal. The maximum material removal and surface roughness were obtained at high waterjet pressure and abrasive mass flow rate. Increasing the abrasive flow rate increased the material removal rate and the surface roughness. Bhandarkar et al. [8] indicated that increased levels of traverse speed and low pressure were beneficial settings for improved cut surface roughness. Begic et al. [9] investigated the influence of AWJM input parameters on the Surface Roughness (SR) of Aluminium. The results showed that increasing material thickness leads to a larger surface roughness value, particularly near the bottom region.

Singh et al. [10] examined the impact of AWJM parameters such as WP, AFR, TS, and SoD on the Material Removal Rate (MRR) and SR of austenitic stainless steel 304. According to the study results, TS is the most significant parameter on MRR and SR; however, stand-off distance was the minimum key parameter in the outcomes. Loschnera et al. [11] exhibited an evaluation of AWJM machining parameter responses in reducing roughness in the straight-cut surface of AISI316l with 10 mm thickness. The experiment results showed that increasing the cutting speed while lowering the Kinetic Energy (KE) of the abrasive particles resulted in noticeable roughness in the bottom cut region. As a result, a slower cutting speed prevents the abrasive waterjet from losing kinetic energy, resulting in a superior surface cut quality. Karthik et al. [12] explored the effects of WP, TF, and AFR on the MRR and kerf width in stainless steel 304 using AWJM. The investigation showed increased water pressure and feed rate values resulted in higher material removal rates. Rao et al. [13] performed abrasive waterjet machining of aluminium AL6061. This study discovered that traverse speed had a stronger effect on surface roughness, whereas WP was the utmost important factor for MRR. Wang et al. [14] revealed the consequence of drilling variables on the Depth of Cut (DoC) and SR in stainless steel abrasive waterjet machining. The experiments were carried out with variable WP, nozzle speed, SoD, and AFR. When the water pressure was increased, the jet's KE increased, resulting in a greater DoC. The higher AFR resulted in greater cutting capabilities of the jet. Azmir et al. [15] experimental results indicated that with the exception of abrasive size, increasing the levels of process parameters led to an increase in the workpiece's surface roughness. Higher mesh-size abrasives produced reduced surface roughness, whereas smaller mesh-size abrasives produced higher roughness while conducting experiments on SS 304 using AWJM. Chen et al. carried out abrasive waterjet cutting on steel EN 1.4306 with a thickness of 20 mm. It was observed from the results that increased WP increased the depth of the hardened layer and the maximum surface hardness. SR at the cut entrance area is substantially better than roughness in the lower cut finishing area, regardless of waterjet pressure.

Kumar et al. [16] investigated the impacts of abrasive waterjet drilling process variables on the Glass Fiber Reinforced Polymer (GFRP) kerf taper, namely WP, TS, and SoD. The experiments were designed using the Taguchi technique, and ANOVA examined the responses. According to the experiment results, traverse speed and hydraulic pressure were the main emerging factors on the kerf taper. Raja et al. [17] experimented to enhance the drilling process for GFRP composites. The experiment was designed using Taguchi, and the ANOVA approach was used to examine the influence of drilling settings on different GFRP specimens. The experiment determined that increased spindle speed resulted in a large reduction in thrust force, but as feed increased, the thrust force and delamination also increased.

The traditional Taguchi approach has been widely used in manufacturing to solve various optimization challenges. This

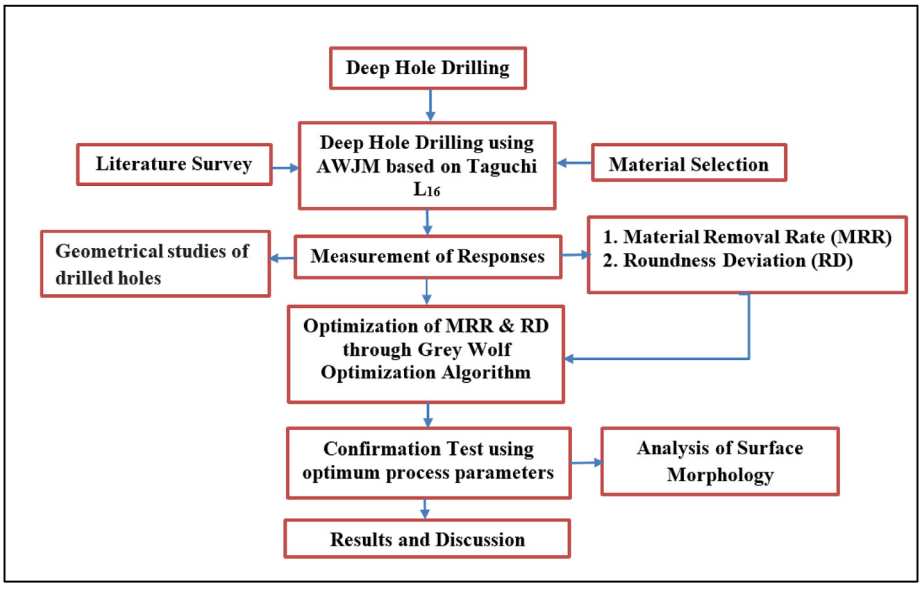

Fig. 1 – Schematic layout of deep hole drilling experimentation and optimization.

strategy substantially improves when dealing with a single variable but could be more effective when dealing with optimization problems with several variables. As a result, TOPSIS, satisfaction function method, grey rational analysis, utility theory, and other methods for optimizing multiple responses have been coupled with the Taguchi techniques [18,19]. The optimization issues were overcome by building mathematical models representing a link between input variables and output responses. Scholars created and used various optimization techniques to solve such mathematical models, including simulated annealing, particle swarm optimization, and genetic algorithms [20,21].

Chohan et al. [22] applied a naked mole-rat algorithm (NMRA) to optimize the process parameters for fused filament fabrication. According to the study, the selected algorithm yielded the best results in improving tensile strength, impact strength, and flexural strength. Fuse et al. [23] used fuzzy AHP and fuzzy TOPSIS methods to optimize the Ti6Al4V alloy process parameters. The results of this study proved that fuzzy logic was an effective technique to optimize the machining parameters. Singh et al. [24] developed two different approaches, namely Generalized Regression Neural Network (GRNN) and Gaussian Process Regression (GPR) for blind hole machining parameter optimization. This study reported that GPR yielded the best results for all responses compared to GRNN. Usca et al. [25] developed a fuzzy interference model to predict the energy conception during the machining of ceramic-based composite. The developed model efficiently reduced by 20% time, energy, and labour.

The studies mentioned above mostly concerned composite and high-strength materials, including Inconel and titanium alloys. There needs to be more experimental and multi-objective optimization work on stainless steel material, namely SS 316L, used in the automobile and medical industries. As a result, there is a scope for further research into the importance of Abrasive Waterjet Drilling (AWJD) process parameters in making high-quality holes in AWJD on SS AISI 316L. This research evaluated the AWJD parameters and their impact on the MRR and RD. Furthermore, the AWJD parameters are improved by utilizing the Grey Wolf Optimization algorithm to enhance MRR while minimizing RD.

Table 1 – Mechanical and chemical properties of SS AISI 316L [27].

Physical	Chemical (in %)
Density - 8.03 (g/cm$^{3)}$	Cr: 16–18%
Yield Strength - 205 (MPa)	Ni: 10–14%
Tensile strength - 515 (MPa)	Mo: 2.0%
Melting Point - 1370–1398 (°C)	N: 0.10%
Specific Heat Capacity - 502 (j/kg-k)	Fe: Bal.

2. Material and methods

2.1. *Selection of material*

Recent advancements in component downsizing and miniaturization have emphasized the demand for deep-hole drilling with a high aspect ratio. The significance of this is evident in the automotive sector, where it is employed for the manufacture of fuel injectors, as well as in the medical field, where it is utilized for the production of bone screws and surgical instruments. The Stainless steel SS AISI 316L material has been selected for deep-hole drilling experimentation, which finds applications in automobile fuel injector bodies. The selected material possesses the following characteristics: excellent durability, resistance to heat and corrosion, minimal maintenance, hardness, and fabrication flexibility. Due to their high alloying content, stainless steels are often more difficult to manufacture. The key issues with traditional Stainless Steel machining include excessive hardening, poor chip formation, the use of numerous tools with varied tool

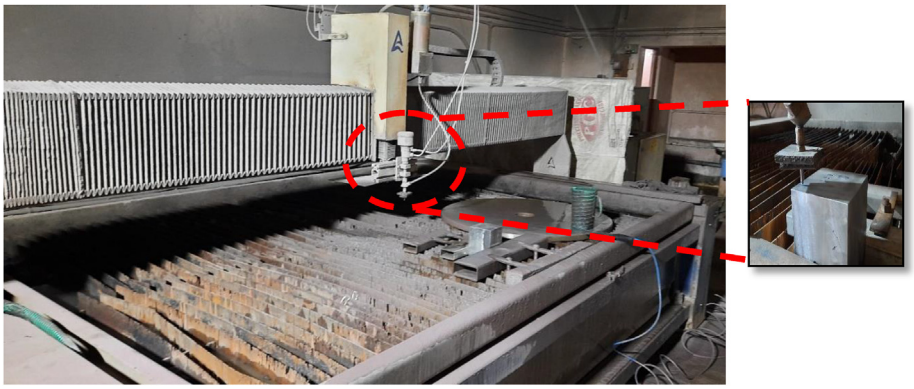

Fig. 2 – Typical abrasive waterjet machine.

Table 2 – AWJD Process parameters and their levels for L_{16} orthogonal array.

Parameters/Levels	1	2	3	4
Water Pressure (MPa)	260	310	335	360
Stand-off distance (mm)	1	1.5	2	2.5
Abrasive mass flow rate (kg/min.)	0.3	0.4	0.5	0.6

geometry, and a huge coolant supply while machining [26]. The schematic layout of deep hole drilling experimentation and optimization is shown in Fig. 1.

SS AISI 316L of 100x100x135 mm is selected as the workpiece material in this experimental work. Many studies have shown the benefits of employing stainless steel in automotive, medical, aerospace, and other industrial applications. Table 1 details the elemental composition of SS AISI 316L.

2.2. *Experimental setup*

Deep hole drilling was carried out on the chosen material using a Gantry waterjet machine tool outfitted with a high-pressure intensifier pump powered by a 60 HP motor capable of delivering an extreme water pressure of 400 MPa. The garnet of size 80 mesh is considered for this study. The deep holes are made through the piercing operation. The typical AWJM experimental setup is shown in Fig. 2. The drilling parameters and their levels are fixed based on pilot research findings and previous literature [28–30]. The experiment's input parameter levels and ranges are based on the AWJD specifications and the optimal parametric range for SS 316L. Based on the variable machining parameters, 16 test runs are designed for the deep hole drill making using the Taguchi L_{16} orthogonal array presented in Table 2.

2.3. *Measurement methods*

This research study includes deep hole drilling features such as piercing time, hole diameter, and roundness.

2.3.1. *Piercing time*

Two approaches were employed to record the time it took to drill each deep hole during the deep hole-making process. The first method employs a standard stopwatch, while the second

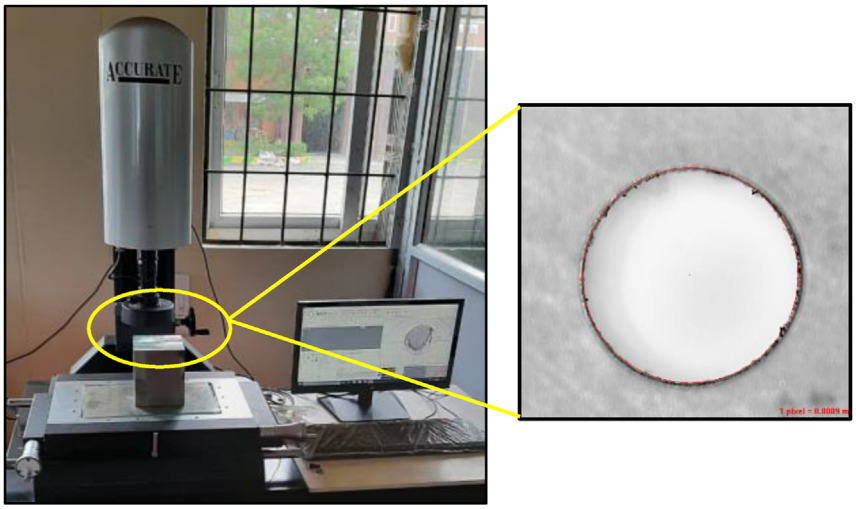

Fig. 3 – Measurement of drilled hole diameter.

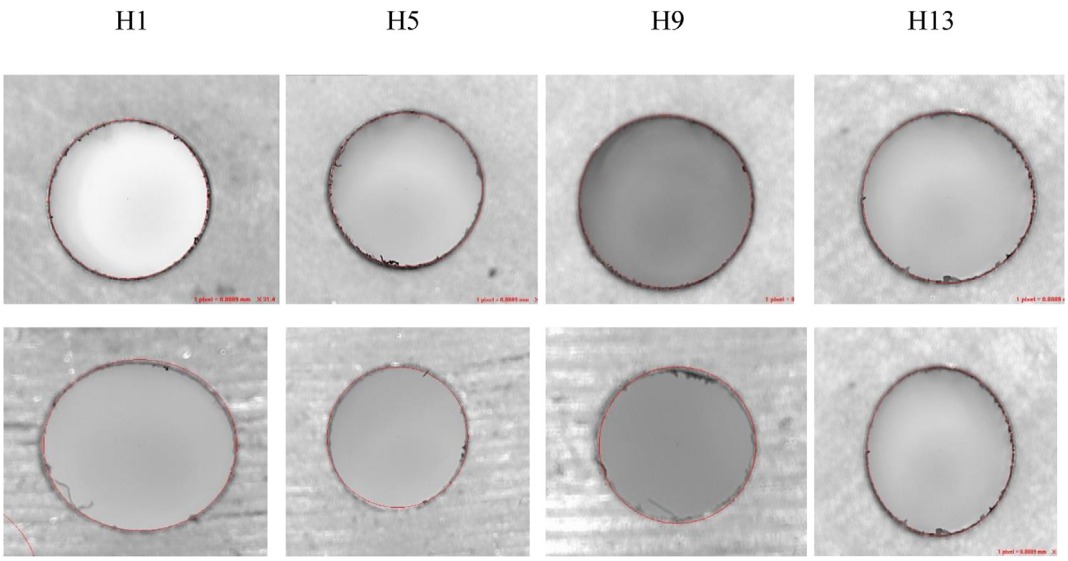

Fig. 4 – Representative image of deep hole diameters measured through VMM.

employs a system that records time. A CNC controller can set the time at the start of the process. The time measurement ambiguity was found to be 0.1s. Drilling time was calculated until the jet pierced the target material's bottom side.

2.3.2. *Geometrical studies of drilled holes*

The measurement of entry and exit diameters of drilled holes using a typical Video Measuring Machine (VMM) is shown in Fig. 3 with a table size of 400 mm × 220 mm. The representative pictures of the entry and exit diameters of Hole no. 1, 5, 9, and 13 are depicted in Fig. 4.

2.3.3. *Material removal rate*

The material removal rate is estimated using the mathematical procedure shown in Equations (1) and (2).

$$MRR = \frac{VMR}{T} \tag{1}$$

$$VMR = 1/3\pi\left(r_{entry}{}^2 + [r_{entry} \times r_{exit}] + r_{exit}{}^2\right)h \tag{2}$$

Where MRR represents material removal rate, VMR refers to the volume of the material removed during drilling. r_{entry} & r_{exit} - radius of entry and exit diameters of the drilled hole in mm, h refers to the thickness of the material in mm, and T refers to the time taken to drill each hole.

2.4. *Experimental outcomes and examination*

To perform the drilling tests on the selected SS AISI 316L specimen, multiple combinations of process control settings according to the L_{16} orthogonal array are configured on AWJD. In addition, the values of MRR and RD are recorded based on the procedure explained in the preceding section. The outcomes of the research are presented in Table 3.

To establish the statistical significance of machining parameters, Minitab software was used to conduct an Analysis of Variance (ANOVA) on the data presented in Tables 4 and 5. The ANOVA findings show that MRR and RD models have P-values below 0.05. As a result, all of the input factors considered in this study are statistically significant.

Table 3 – Drilling parameters and outcomes of AWJD.

Sl.No.	WP (MPa)	SoD (mm)	AFR (g/min.)	MRR (mm^3/min.)	RD (mm)
1.	260	1	0.3	27.57	0.48
2.	260	1.5	0.4	30.33	0.41
3.	260	2	0.5	30.89	0.80
4.	260	2.5	0.6	26.66	1.07
5.	310	1	0.4	34.93	0.53
6.	310	1.5	0.3	36.37	0.63
7.	310	2	0.6	35.37	0.82
8.	310	2.5	0.5	34.19	1.20
9.	335	1	0.5	39.73	0.80
10.	335	1.5	0.6	37.40	0.70
11.	335	2	0.3	36.68	0.89
12.	335	2.5	0.4	36.78	0.93
13.	360	1	0.6	42.51	0.61
14.	360	1.5	0.5	58.23	0.59
15.	360	2	0.4	40.33	0.62
16.	360	2.5	0.3	42.25	0.80

Table 4 – ANOVA for material removal rate.

Source	DF	Adj SS	Adj MS	F-Value	P-Value
Regression	9	889.860	98.8734	17.25	0.001
WP	1	53.502	53.5020	9.34	0.022
SoD	1	12.149	12.1491	2.12	0.196
AFR	1	0.070	0.0696	0.01	0.916
WP*WP	1	83.575	83.5748	14.58	0.009
SoD*SoD	1	58.906	58.9056	10.28	0.018
AFR*AFR	1	47.679	47.6790	8.32	0.028
WP*SoD	1	10.643	10.6429	1.86	0.222
WP*AFR	1	6.429	6.4291	1.12	0.330
SoD*AFR	1	41.585	41.5845	7.26	0.036
Error	6	34.385	5.7308		
Total	15	924.245			

Table 5 – ANOVA for roundness deviation.

Source	DF	Adj SS	Adj MS	F-Value	P-Value
Regression	9	0.620202	0.068911	19.58	0.001
WP	1	0.075633	0.075633	21.49	0.004
SoD	1	0.004046	0.004046	1.15	0.325
AFR	1	0.008524	0.008524	2.42	0.171
WP*WP	1	0.070057	0.070057	19.91	0.004
SoD*SoD	1	0.071423	0.071423	20.30	0.004
AFR*AFR	1	0.000856	0.000856	0.24	0.639
WP*SoD	1	0.032240	0.032240	9.16	0.023
WP*AFR	1	0.007605	0.007605	2.16	0.192
SoD*AFR	1	0.001065	0.001065	0.30	0.602
Error	6	0.021114	0.003519		
Total	15	0.641316			

The Pareto charts shown in Fig. 5(a–d) are used to systematically evaluate the impact of AWJD process variables on MRR and RD. The AWJD process variables, notably WP and AFR, have the maximum influence on the MRR value. Similarly, the most influential criteria in determining the RD value are WP and SoD. In addition, the residual distribution values for both responses are shown in Fig. 5(e–f). These findings show that the drilling parameters were appropriately selected to maximize MRR and minimize RD.

Additionally, regression models for MRR and RD are generated with the programme Minitab™ based on the correlation among AWJD process variables and responses. These models are used to predict MRR and RD values. Equations (3) and (4) yield the regression equations for MRR and RD, respectively.

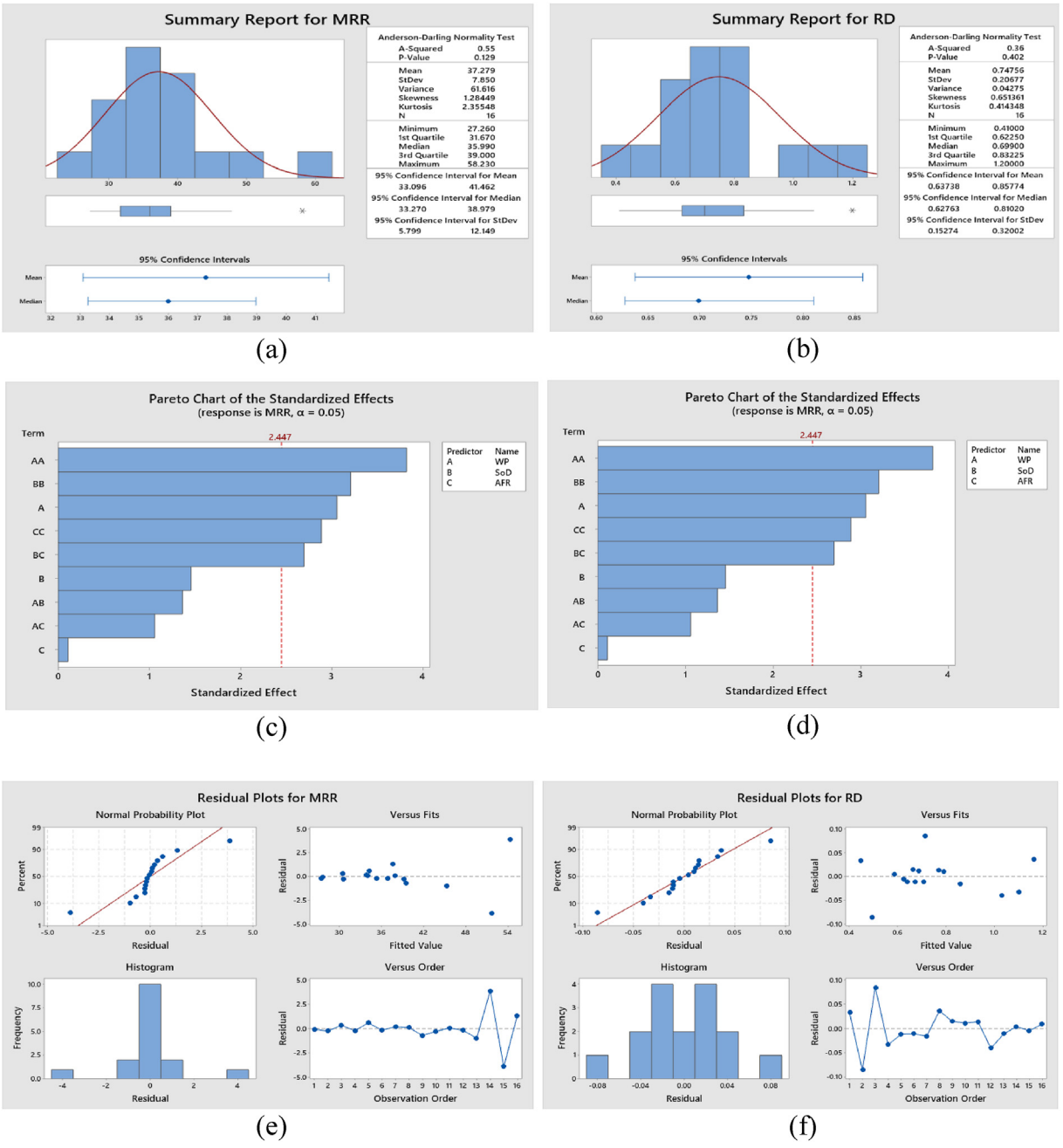

Fig. 5 – (a–f) Statistical significance of MRR and RD.

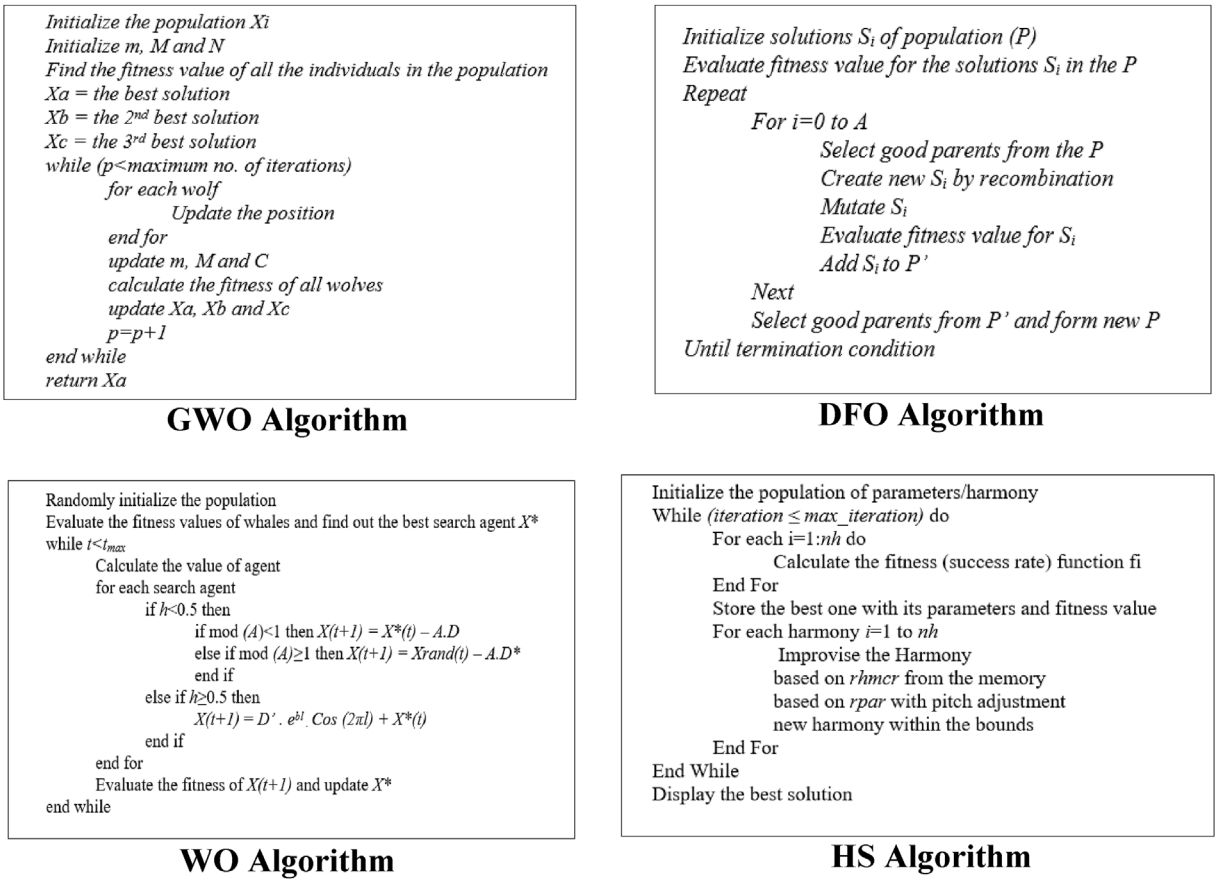

Fig. 6 – Pseudocode of optimization algorithms.

Table 6 – Optimum process control parameters through the GWO Algorithm.

Algorithm	WP (MPa)	SoD (mm)	AFR (kg/min.)
Grey Wolf Optimization Algorithm	260.8708	1.549062	0.371789

Table 7 – Responses obtained through GWO Algorithm.

Algorithm	MRR (mm^3/min.)	RD (mm)
Grey Wolf Optimization Algorithm	31.08641	0.55253

Table 9 – Quality indicators for comparing Algorithm's performance.

Algorithm	IGD	SP
GWO	0.057929	0.005718
DFO	0.087900	0.006507
WO	0.162863	0.011324
HS	0.098220	0.047814

$$MRR = 8.2 - 1.097\,WP + 30.2\,SOD - 12\,AFR + 0.002150\,WP*WP - 7.68\,SOD\,SOD*\,SOD - 172.6\,AFR*AFR - 0.0720\,WP*SOD + 0.280\,WP*AFR + 42.8\,SOD*AFR \quad (3)$$

Table 8 – Optimum process parameters and their responses.

Algorithm	WP (MPa)	SoD (mm)	AFR (g/min.)	MRR (mm^3/min.)	RD (mm)
GWO	260.8708	1.549062	0.371789	31.08641	0.55253
DFO	261.8208	1.531507	0.365979	31.04591	0.555698
WO	269.1592	1.428741	0.361969	30.92208	0.562645
HS	272.534	1.421662	0.398524	30.94148	0.559698

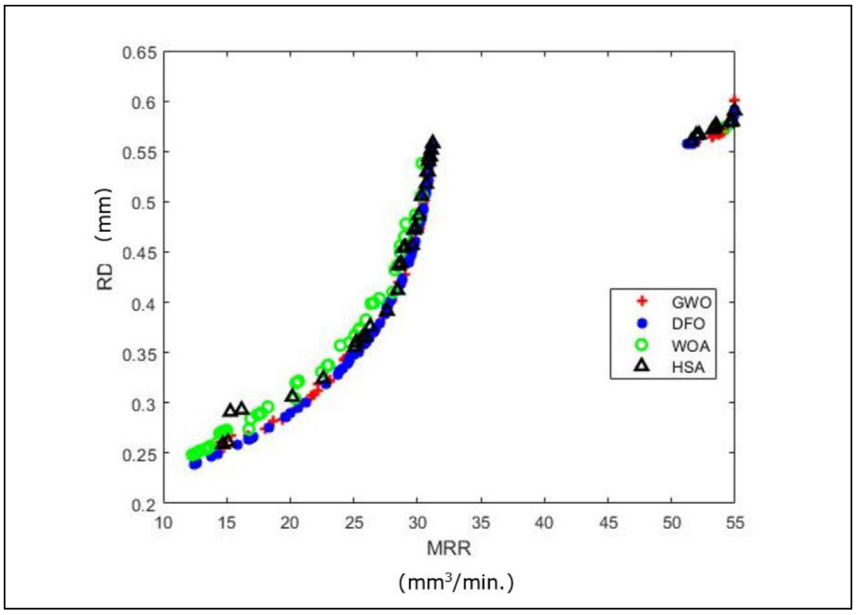

Fig. 7 – Pareto front diagram for MRR vs. RD.

$$RD = 5.51 + 0.04125\,WP + 0.550\,SOD - 4.11\,AFR - 0.000062 + 0.2672\,SOD * SOD + 0.73\,AFR * AFR - 0.00397\,WP * SOD + 0.00963\,WP * SOD + 0.216\,SOD * AFR \quad (4)$$

3. Results and discussion

3.1. *Algorithmic method*

This study uses the Grey Wolf Optimization method to identify the best AWJM machining settings for concurrently maximizing the MRR and minimizing the RD values. The GWO algorithm has several advantages over other methods as follows: (i) The idea of social hierarchy enables GWO to store the best solutions after each iteration (ii) The search space near the prey can be expanded to numerous dimensions as required by the optimization issue (iii) The random parameters support the prospective solutions in seeking and searching for prey by encircling around them (iv) It simply has two variable parameters as described by Chakraborty et al. [31] and Mirjalili et al. [32].

In addition, the GWO algorithm's efficacy in this work is compared to the Derivative-Free Optimization (DFO), Whale Optimization (WO), and **Harmony Search (HS)** algorithms.

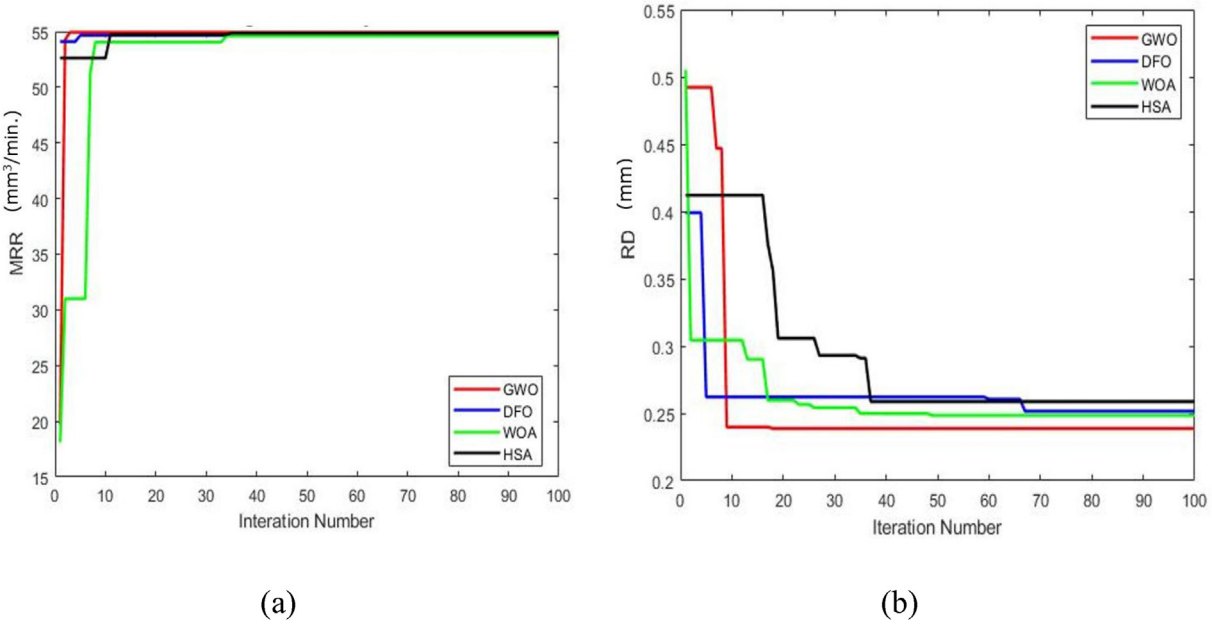

Fig. 8 – Convergence graph (a) MRR (b) RD.

Table 10 – Outcomes of the validation experiment.

AWJD Parameters		MRR (mm^3/min.)			RD (mm)		
Description	Value	GWO Algorithm	Exp. value	% of deviation	GWO Algorithm	Exp. value	% of deviation
WP	260.870						
SD	1.549	31.086	30.330	2.49	0.552	0.545	1.28
FR	0.371						

Fig. 6 depicts the pseudocode for all of the algorithms. The optimal process control parameters are determined using the aforementioned algorithms, and the associated results are reported in Tables 6 and 7.

Table 8 displays the appropriate outcomes from applying the algorithms to determine the optimal process control settings. Furthermore, the algorithm's performance is compared using Spacing (SP) and Inverted Generational Distance (IGD). Finally, Table 9 shows the performance of algorithms based on the measures.

The Pareto front diagram for MRR vs. RD shown in Fig. 7 revealed that the GWO algorithm outperformed others. Further, the convergence plots for MRR and RD shown in Fig. 8 demonstrated the GWO algorithm's efficacy. As a result, the GWO algorithm outperformed DFO, WO, and HS algorithms. The validation experimentation was also carried out utilizing the GWO algorithm and the ideal combination of AWJD parameter settings. The outcomes of the validation run and the variation in percentage from the GWO algorithm are presented in Table 10.

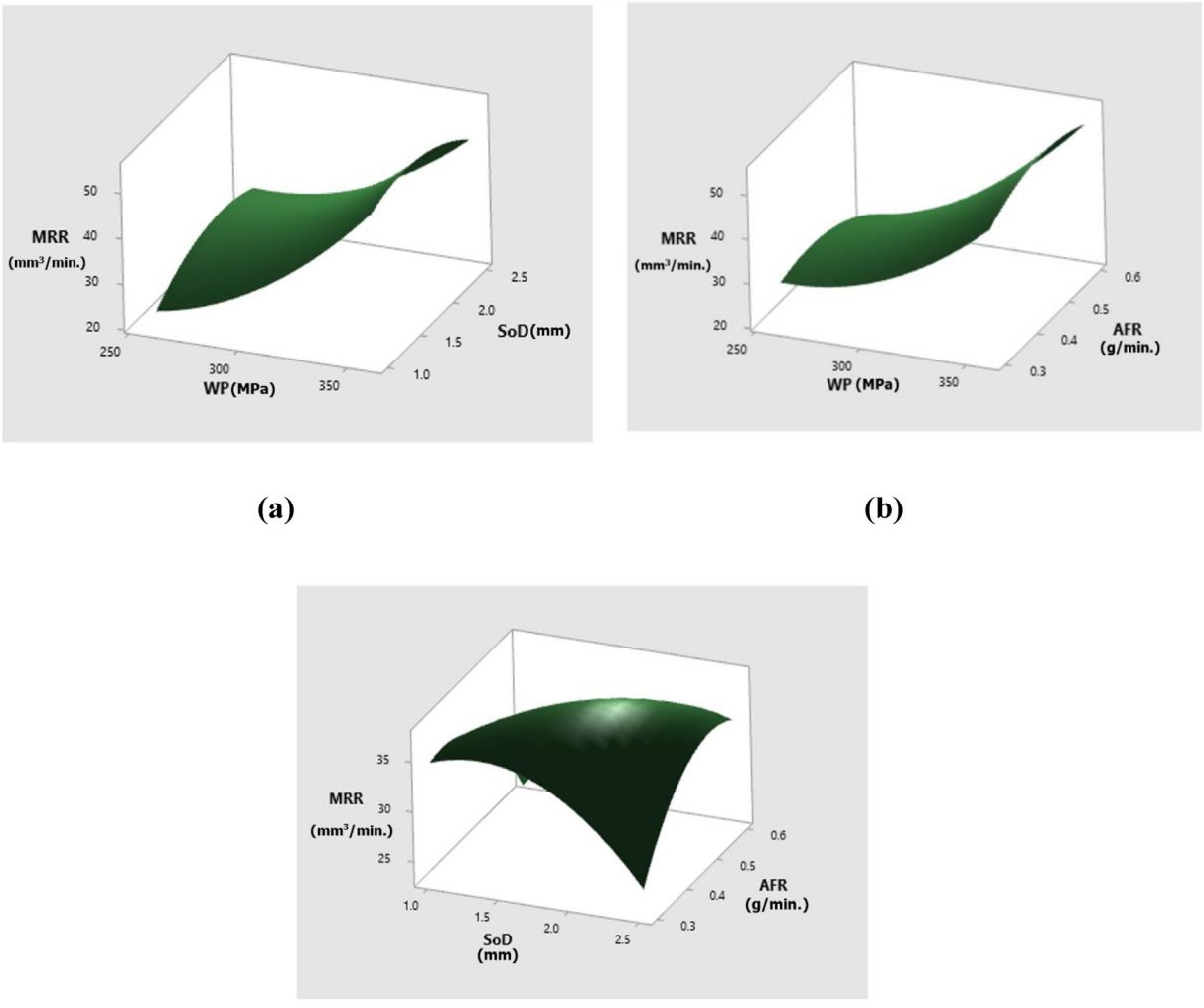

Fig. 9 – (a–c) 3D Surface plot for the impact of AWJD process parameters on MRR.

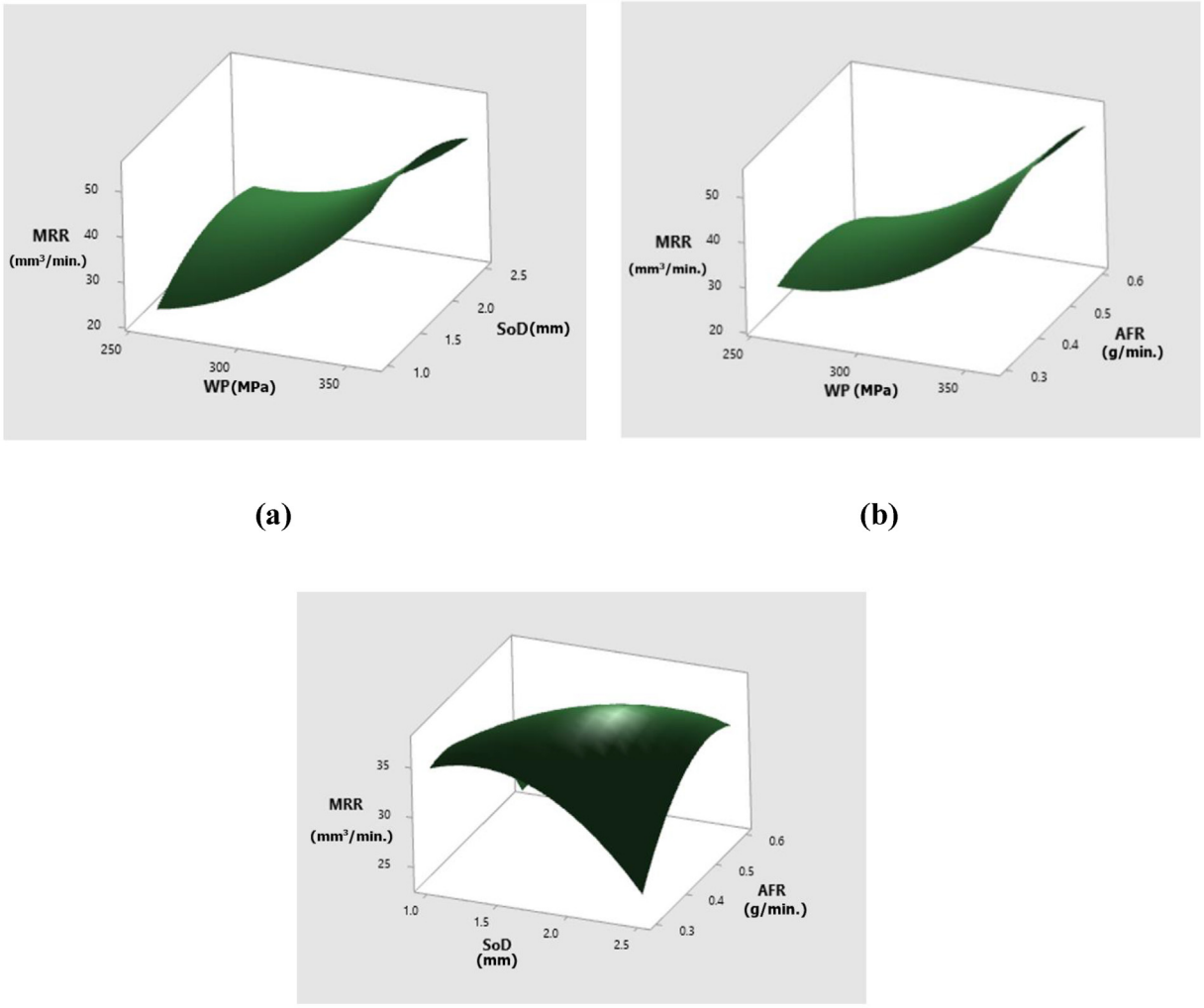

Fig. 10 – (a–c) 3D surface plot for the effect of AWJD process parameters on RD.

3.2. *Impact of AWJD drilling parameters on MRR*

During machining operations, the amount of material removed substantially impacts the processing cost and pace of output. As a result, industries are always seeking ways to enhance MRR to fulfil demand while minimizing production costs.

According to the statistical study, the process factors studied substantially impact the MRR of the deep hole drilling process. As a result, it is critical to explore these components' interactions to comprehend the MRR mechanism during deep-hole drilling. A 3D surface plot Fig. 9 (a) illustrates the effect of WP and SoD on the MRR. As seen in the plot, increasing the WP increased the MRR greatly. The abrasive jet's severe impact erodes the target material's surface. The velocity of a waterjet is assumed to be proportional to the square root of the WP. Because the KE level of the jet increases with pressure, the penetration rate and, subsequently, the material removal rate increase.

Fig. 9 (b) illustrates the effect of WP and AFR on MRR. The cohering action produced by the collisions of a great number of abrasive particles in the direction of the workpiece is principally responsible for the processing of AWJM [33]. Furthermore, the degree of material removal is related to the AFR and the pressure of the waterjet. It is well understood that an increase in AFR tends to increase the MRR as more abrasive particles are available to strike the target material with enormous force, resulting in a greater material removal rate.

Increases in waterjet pressure cause greater kinetic energy, accelerating the erosion or cutting rate and removing more material from the specimen [34]. As a result, waterjet pressure plays a pivotal role in determining the material removal rate. As the distance from the nozzle tip increases, the diameter of the abrasive jet continuously widens owing to scattering, lowering the particle velocity and MRR. Because the kinetic energy supplied by the abrasive particles is employed to erode material from the work surface progressively, increased stand-off distance results in lesser penetration and reduced

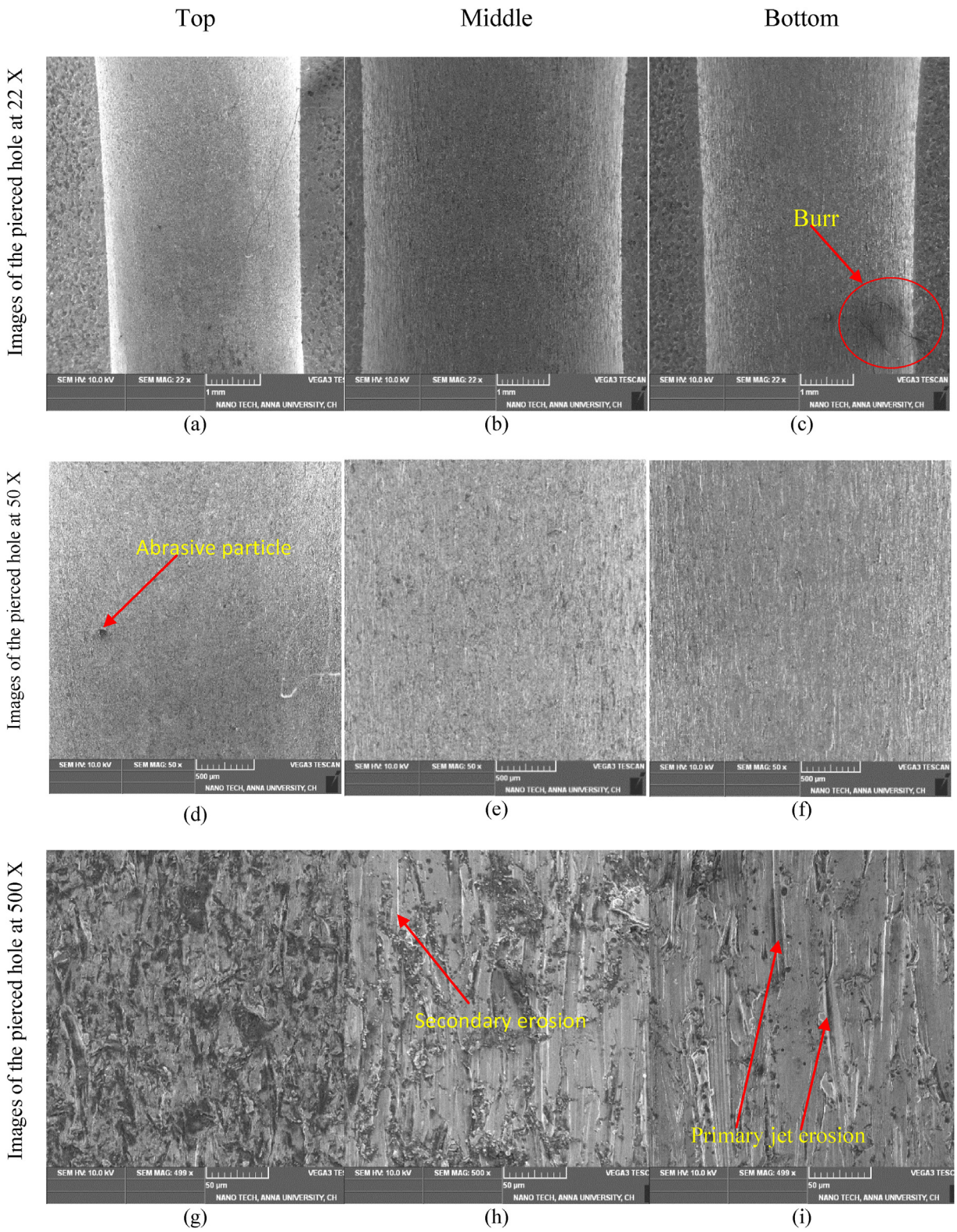

Fig. 11 – SEM image of deep holes at the top, middle, and bottom under different magnifications.

MRR. Nevertheless, if the stand-off distance is even small, there will be insufficient clearance for the used abrasive particles to exit the drilling region later impact. It can significantly limit the velocity of a new jet due to collision, resulting in reduced efficacy of the jet in terms of material erosion. As a result, the SoD increases both the MRR and penetration rise progressively, but, at a certain limit, both decline with further increase in SoD, as shown in Fig. 9 (c).

3.3. *Impact of AWJD process parameters on roundness deviation*

In this investigation, roundness deviation was chosen as an additional quality criterion affecting the geometric correctness of the AWJM drilled holes. Roundness measures an object's resemblance to a mathematically perfect circle [35]. Roundness is associated with two dimensions: cross-sectional circles and cylindrical items. The roundness inaccuracy is expressed by the maximum and minimum diameters variance at the hole's entrance and exit [36]. The roundness deviation of the drilled holes was measured by the Vision measuring machine (make: Accurate, Model: VPP-ME 2010).

According to Fig. 10 (a & b), it is observed that RD is reduced while drilling at increased WP. Increasing WP showed a substantial favourable effect on RD reduction. The impact of WP and AFR is even more on roundness deviation. When the water pressure is raised, the jet's kinetic energy rises, resulting in a strong momentum transfer of the abrasive particles. As a result, the difference in the formation of maximum and minimum diameters is minimized, resulting in a decrease in RD.

The influence of SoD on RD is demonstrated in Fig. 10 (c). The diameter of the waterjet formed by abrasive particles as it exited the nozzle increased as SoD increased, which increased the RD. According to the graph, increasing SoD in SS 316L deep hole drilling operations reduces dimensional stability and increases RD values. This is attributed to increased waterjet diameter produced by increased SoD, which resulted in lower abrasive concentration and differences in top and bottom surface hole sizes [37].

3.4. *Microstructure analysis of drilled hole*

The drilled surfaces generated during AWJM deep hole drilling of SS 316L through optimum process parameters are topographically illustrated in Fig. 11 responses to the application of WP, SoD, and AFR. The deep hole surfaces at the drilled holes' top, middle, and bottom were examined using a Scanning Electron Microscope (SEM) to determine the material removal pattern.

Fig. 11 depicts the low-magnification images of these three locations in a newly drilled hole (a-c). Fig. 10 (a) and (b) show that the top and middle parts have smooth drilled surfaces, unlike the bottom section in Fig. 11 (c). The optimum process parameter of WP 260 MPa, SoD 1.5 mm, and AFR 0.3 g/min. It produced better machining surfaces at the top and middle of the drilled specimen. This indicates that low WP and AFR generate sufficient cutting force compared to higher waterjet pressure with the same abrasive, leading to the development of the critical force. This was achieved because fine abrasive particles in the garnet of mesh size #80 with a low abrasive mass flow rate produced a uniform penetration effect at the top and middle of the drilled hole; as a result, defect-free surfaces were obtained. When the depth of the workpiece increases, the kinetic energy of the waterjet decreases, and as a result, slightly poor drilled surfaces at the bottom of the workpiece are visible. This is because of the low kinetic energy of the waterjet and abrasive particles to drill the surfaces with uniform penetration.

The SEM images of medium and high magnification from the top, middle, and bottom sections are revealed in Fig. 11(d–f) and (g-i), respectively. These images depict material removal characteristics, such as primary and secondary jet erosion. Plowing is the primary jet material removal method in which an impinging high-velocity waterjet with abrasives scoops up material along the jet's flow path. The ploughing action leaves a mark that is narrow in width but deep in depth and perfectly straight in the direction of the jet's movement. However, secondary erosion occurs due to the broken abrasive particles in the back-bouncing jet, which remove material by erosive action.

In contrast to the primary material removal mechanism, which leaves a deeply aligned trace along the jet direction is seen in Fig. 11(e–f). In comparison to primary material removal, secondary removes less material. In addition, Abrasive particles and burrs have also been found to embed notably in the middle sections and might be attributed to jet turbulence caused by the counter-action between the incoming and back-bouncing jets.

4. Conclusion

Using the L_{16} orthogonal array, deep hole drilling was performed on SS 316L material to study the effects of different AWJM parameter combinations. The experiment results were noted and statistically evaluated with ANOVA. Minitab was used to establish relationships between AWJM parameters and MLRM equations for MRR and RD. GWO algorithm was applied to find the ideal AWJD process parameters to maximize MRR and minimize RD. The GWO algorithm's efficacy was also compared to that of the DFO, WO, and HS algorithms. This investigation led to the following observations.

1. The WP and AFR directly impact MRR; greater waterjet pressure produces more kinetic energy, resulting in a quicker erosion or cutting rate and more material eroded off the workpiece. An increase in AFR tends to increase the MRR as more abrasive particles are available to strike the target material with enormous force, resulting in a greater material removal rate.
2. The SoD has the reverse effect on the MRR because the distance from the nozzle tip increases, the diameter of the abrasive jet gradually expands due to spreading, and the velocity of the abrasive particles decreases.
3. Increased WP greatly reduces the RD because the variations in the formation of diameters were strongly controlled by waterjet pressure. However, increased SoD tends to increase the RD.
4. The analysis of variance revealed that WP and AFR were the two most influential AWJD parameters in determining the MRR value. The most significant factors in establishing the RD value were WP and SoD.
5. The suggested GWO algorithm generated the ideal AWJM process variables for maximizing the MRR and minimizing

the RD values, as measured by diversity and spacing, demonstrating its superiority over the DFO, WO, and HS algorithms.

6. According to the GWO algorithm, the optimal set of process parameters for AWJD deep hole drilling has MRR values of 31.08 mm^3/min and RD values of 0.55 mm, respectively.
7. The confirmation experiment yielded MRR and RD values of 30.33 mm^3/min and 0.545 mm, with corresponding variances of 2.49% and 1.28%.
8. SEM images revealed that the deep hole surfaces are fairly smooth, and ploughing action was discovered to be the major mechanism of material removal, but secondary erosion occurred at the intermediate portion in addition to ploughing due to jet turbulence caused by the counteraction between the incoming and returning jets.

Declaration of competing interest

We have no conflict of interest.

Acknowledgement

This work was supported by Qatar National Research Fund under the grant no. MME03-1226-210042. The statements made herein are solely the responsibility of the authors.

Nomenclature

AWJM	Abrasive Waterjet Machine
GWO	Grey Wolf Optimization
WP	Waterjet Pressure
AFR	Abrasive Mass Flow Rate
SoD	Stand-off Distance
TS	Traverse Speed
KE	Kinetic Energy
SR	Surface Roughness
MRR	Material Removal Rate
DoC	Depth of Cut
GFRP	Glass Fiber Reinforced Polymer
AWJD	Abrasive Waterjet Drilling
VMR	Volume of material removed
ANOVA	Analysis of Variance
RD	Roundness Deviation
DFO	Derivative-Free Optimization
WO	Whale Optimization
HS	Harmony Search
SP	Spacing
IGD	Inverted Generational Distance

REFERENCES

[1] Momber AW, Kovacevic R. Principles of abrasive water jet machining. London, England: Springer; 2012.
[2] Natarajan Y, Murugesan PK, Mohan M, Liyakath Ali Khan SA. Abrasive water jet machining process: a state of art of review. J Manuf Process 2020;49:271–322. https://doi.org/10.1016/j.jmapro.2019.11.030.
[3] Hlavacova IM, Sadilek M, Vanova P, Szumilo S, Tyc M. Influence of steel structure on machinability by abrasive water jet. Materials 2020;13(19):4424. https://doi.org/10.3390/ma13194424.
[4] Kowsari K, Nouraei H, James DF, Spelt JK, Papini M. Abrasive slurry jet micro-machining of holes in brittle and ductile materials. J Mater Process Technol 2014;214(9):1909–20. https://doi.org/10.1016/j.jmatprotec.2014.04.008.
[5] Llanto JM, Tolouei-Rad M, Vafadar A, Aamir M. Recent progress trend on abrasive waterjet cutting of metallic materials: a review. Appl Sci (Basel) 2021;11(8):3344. https://doi.org/10.3390/app11083344.
[6] Kantha Babu M, Krishnaiah Chetty OV. A study on recycling of abrasives in abrasive water jet machining. Wear 2003;254(7–8):763–73. https://doi.org/10.1016/s0043-1648(03)00256-4.
[7] Veerappan G, Ravichandran M. Experimental investigations on abrasive water jet machining of nickel-based superalloy. J Braz Soc Mech Sci Eng 2019;41(11). https://doi.org/10.1007/s40430-019-2031-1.
[8] Bhandarkar V, Singh V, Gupta TVK. Experimental analysis and characterization of abrasive water jet machining of Inconel 718. Mater. Today Off 2020;23:647–50. https://doi.org/10.1016/j.matpr.2019.04.227.
[9] Begic-Hajdarevic D, Cekic A, Mehmedovic M, Djelmic A. Experimental study on surface roughness in abrasive water jet cutting. Procedia Eng 2015;100:394–9. https://doi.org/10.1016/j.proeng.2015.01.383.
[10] Singh D, Chaturvedi V. Investigation of optimal processing condition for abrasive water jet machining for stainless steel AISI 304 using grey relational analysis coupled with S/N ratio. Appl Mech Mater 2014;592–594:438–43. https://doi.org/10.4028/www.scientific.net/amm.592-594.438.
[11] Loschner P, Jarosz K, Niesłony P. Investigation of the effect of cutting speed on surface quality in abrasive water jet cutting of 316L stainless steel. Procedia Eng 2016;149:276–82. https://doi.org/10.1016/j.proeng.2016.06.667.
[12] Karthik K, Smith Sundarsingh D, Harivignesh M, Gopi Karthick R, Praveen M. Optimization of machining parameters in abrasive water jet cutting of stainless steel 304. Mater Today 2021;46:1384–9. https://doi.org/10.1016/j.matpr.2021.02.489.
[13] Rao MS. Parametric optimization of abrasive waterjet machining for mild steel: Taguchi approach. Int. j. curr. eng. technol. 2013;2(2):28–30. https://doi.org/10.14741/ijcet/spl.2.2014.06.
[14] Wang J, Wong WCK. A study of abrasive waterjet cutting of metallic coated sheet steels. Int J Mach Tool Manufact 1999;39(6):855–70. https://doi.org/10.1016/s0890-6955(98)00078-9.
[15] Azmir MA, Ahsan AK. Investigation on glass/epoxy composite surfaces machined by abrasive water jet machining. J Mater Process Technol 2008;198(1–3):122–8. https://doi.org/10.1016/j.jmatprotec.2007.07.014.
[16] Kumar UA. Optimization of kerf width & kerf taper angle on Glass fiber reinforced polymer by abrasive water jet machining using Taguchi approach. Int J Res Appl Sci Eng Technol 2019;7(10):445–50. https://doi.org/10.22214/ijraset.2019.10067.
[17] Raja R, Jannet S. Comparative evaluation of drilling on GFRP made by different fabrication techniques. In: Lecture notes on multidisciplinary industrial engineering. Singapore: Springer Singapore; 2020. p. 583–97.
[18] Abhishek K, Datta S, Mahapatra SS. Multi-objective optimization in drilling of CFRP (polyester) composites: application of a fuzzy embedded Harmony search (HS)

algorithm. Measurement 2016;77:222–39. https://doi.org/10.1016/j.measurement.2015.09.015.
[19] Bagada C, Damor H, Prajapati V, Abhishek K. Utility function approach integrated with fuzzy for optimization in milling Glass fiber reinforced epoxy composites. In: Recent advances in mechanical infrastructure. Singapore: Springer Singapore; 2020. p. 85–91.
[20] Abhishek K, Rakesh Kumar V, Datta S, Mahapatra SS. Parametric appraisal and optimization in machining of CFRP composites by using TLBO (Teaching–Learning based optimization algorithm). J Intell Manuf 2017;28(8):1769–85.
[21] Kumari S, Bandhu D, Kumar A, Yadav RK, Vivekananda K. Application of utility function approach aggregated with imperialist competitive algorithm for optimization of turning parameters of AISI D2 steel. In: Recent advances in mechanical infrastructure. Singapore: Springer Singapore; 2020. p. 49–57.
[22] Chohan JS, Mittal N, Kumar R, Singh S, Sharma S, Dwivedi SP, et al. Optimization of FFF process parameters by naked mole-rat algorithms with enhanced exploration and exploitation capabilities. Polymers 2021;13(11):1702. https://doi.org/10.3390/polym13111702.
[23] Fuse K, Dalsaniya A, Modi D, Vora J, Pimenov DY, Giasin K, et al. Integration of fuzzy AHP and fuzzy TOPSIS methods for wire electric discharge machining of titanium (Ti6Al4V) alloy using RSM. Materials 2021;14(23):7408. https://doi.org/10.3390/ma14237408.
[24] Singh SK, Mali HS, Unune DR, Wojciechowski S, Wilczyński D. Application of generalized regression neural network and gaussian process regression for modelling hybrid micro-electric discharge machining: a comparative study. Processes 2022;10(4):755. https://doi.org/10.3390/pr10040755.
[25] Usca ÜA, Şap S, Uzun M, Kuntoğlu M, Salur E, Karabiber A, et al. Estimation, optimization and analysis based investigation of the energy consumption in machinability of ceramic-based metal matrix composite materials. J Mater Res Technol 2022;17:2987–98. https://doi.org/10.1016/j.jmrt.2022.02.055.
[26] Supriya SB, Srinivas S. Machinability studies on stainless steel by abrasive water jet -review. Mater Today 2018;5(1):2871–6. https://doi.org/10.1016/j.matpr.2018.01.079.
[27] Guo P, Zou B, Huang C, Gao H. Study on microstructure, mechanical properties and machinability of efficiently additive manufactured AISI 316L stainless steel by high-power direct laser deposition. J Mater Process Technol 2017;240:12–22. https://doi.org/10.1016/j.jmatprotec.2016.09.005.
[28] Gurusamy S, Nagarajan L, Shanmuga Sundaram Ram P. Experimental study on abrasive water jet machining of AA5083 in a range of thicknesses. Int J Abras Technol 2018;8(3):218. https://doi.org/10.1504/ijat.2018.10015291.
[29] Hocheng H, Tsai HY, Shiue JJ, Wang B. Feasibility study of abrasive-waterjet milling of fiber-reinforced plastics. J Manuf Sci Eng 1997;119(2):133–42. https://doi.org/10.1115/1.2831088.
[30] Muralidharan S, Aatthisugan I, Tripathi A, Baradiya H, Singh A. A study on machinability of polymer composite by abrasive water jet machining. IOP Conf Ser Mater Sci Eng 2018;402:012102. https://doi.org/10.1088/1757-899x/402/1/012102.
[31] Chakraborty S, Mitra A. Parametric optimization of abrasive waterjet machining processes using grey Wolf optimizer. Mater Manuf Process 2018;33(13):1471–82. https://doi.org/10.1080/10426914.2018.1453158.
[32] Mirjalili S, Saremi S, Mirjalili SM, Coelho L, dos S. Multi-objective grey Wolf optimizer: a novel algorithm for multi-criterion optimization. Expert Syst Appl 2016;47:106–19. https://doi.org/10.1016/j.eswa.2015.10.039.
[33] Thamizhvalavan P, Arivazhagan S, Yuvaraj N, Ramesh B. Machinability study of abrasive aqua jet parameters on hybrid metal matrix composite. Mater Manuf Process 2019;34(3):321–44. https://doi.org/10.1080/10426914.2018.1544707.
[34] Llanto JM, Vafadar A, Aamir M, Tolouei-Rad M. Analysis and optimization of process parameters in abrasive waterjet contour cutting of AISI 304L. Metals 2021;11(9):1362. https://doi.org/10.3390/met11091362.
[35] Rathinasuriyan C, Bharani Chandar J, Palanisamy R. Optimization of roundness in plasma arc drilling process by Taguchi approach. Mater Today 2022;52:278–82. https://doi.org/10.1016/j.matpr.2021.08.257.
[36] Sen M, Shan HS. Analysis of roundness error and surface roughness in the electro jet drilling process. Mater Manuf Process 2006;21(1):1–9. https://doi.org/10.1081/amp-200060398.
[37] Prasad KS, Chaitanya G. Selection of optimal process parameters by Taguchi method for drilling GFRP composites using abrasive water jet machining technique. Mater Today 2018;5(9):19714–22. https://doi.org/10.1016/j.matpr.2018.06.333.